Silicon metasurfaces with tunable electromagnetic resonances for nonlinear optical conversion

L. Fagiani([1])([2]), A. Zilli([1]), A. Tognazzi([3])([4]), E. Mafakheri([2]),
K. Okhlopkov([5]), D. Rocco([3])([4]), M. Shcherbakov([5]), A. Fedyanin([5]),
C. De Angelis([3])([4]), M. Finazzi([1]), M. Celebrano([1]) and M. Bollani([2])

([1]) *Department of Physics, Politecnico di Milano - Piazza L. Da Vinci 32,*
   20133 Milano, Italy
([2]) *CNR-IFN, LNESS laboratory - Via Anzani 42, 22100 Como, Italy*
([3]) *Department of Information Engineering, University of Brescia - Via Branze 38,*
   Brescia, Italy
([4]) *CNR-INO - Via Branze 45, 25123 Brescia, Italy*
([5]) *Faculty of Physics, Lomonosov Moscow State University - Moscow 119991, Russia*

Summary. — Dielectric metasurfaces sustain electromagnetic modes which can be exploited to enhance nonlinear frequency-conversion processes such as third-harmonic generation. In this work we employ electron-beam lithography to fabricate silicon metasurfaces supporting electromagnetic resonances with different quality factors (Q), ruled by the geometry. This allows to investigate the trade-off between resonant enhancement and matching the spectral bandwidth of the ultrafast excitation source. Both experiments and simulations indicate that higher values of Q do not *a priori* bring about a stronger third-harmonic generation, which correlates to the spectral overlap between the metasurface resonance and the pump bandwidth.

1. – Introduction

Miniaturizing systems with nonlinear optical functionalities is a major technological challenge, since the efficiency of generating radiation at new frequencies decreases due to the small volume of matter involved. This can be compensated by carefully designing subwavelength systems to support localized electromagnetic resonances [1, 2]. Metasurfaces (MSs) have emerged as powerful tools to achieve such control [3]. They are planar arrays of resonators with footprint comparable to the wavelength of visible light, that is, hundreds of nanometers. Their electromagnetic coupling can mould the flow of light at the nanoscale to perform beam steering [4], focusing [5] and boost nonlinear processes such as second-harmonic generation [6].

Platforms based on high refractive-index dielectric materials are promising for such purposes [7, 8], since they exhibit low losses with respect to their metal counterparts. Silicon (Si) has gained a foothold in nonlinear nanoscale photonics thanks to its well-established fabrication processes [9], high refractive index and strong third-order optical susceptibility [10]. In this scenario, advances in nanofabrication play a key role, inasmuch as the sensitive dependence of the optical resonances on the geometry and material composition offers ample opportunities for controlling the optical properties. Here, we study the third-harmonic (TH) emission of silicon MSs fabricated on a silicon-on-insulator (SOI) substrate by electron-beam lithography (EBL) and reactive ion etching
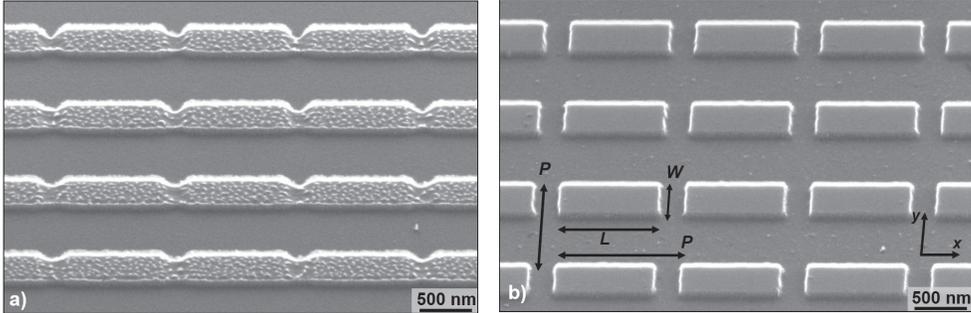
Fig. 1. – 45°-tilted SEM micrographs of exemplary Si MSs ($H = 125$ nm, $L = 981$ nm, $W = 459$ nm, $P = 1117$ nm) fabricated with (a) negative and (b) positive resists.

(RIE). We investigate the effect of the metasurface (MS) design on its optical properties, with particular focus on the effective coupling to the optical excitation in the frequency domain.

2. – Fabrication protocol

The studied MSs are periodic square arrays of Si cuboids of equal height (H), length (L), width (W), and pitches (P) as reported in fig. 1. They were fabricated through a top-down process performed by a combination of EBL and RIE, starting from Si thickness of 125 nm on $2\,\mu$m of SiO$_2$ buried oxide layer [9]. The first sample (fig. 1(a)) was fabricated with a negative resist (AR-N7520), which was spin-coated onto the substrate at 4000 rpm and baked for 1 min at 80 °C. After the exposure, it was developed in AR 400 37 for 50 s at room temperature. Another 1 min treatment at 80 °C was performed to increase the resist stability. RIE was then performed with SF$_6$ gas, with a power of 50 W for 20 s under a 1.06×10^{-4} mbar pressure. The major problem encountered when using a negative resist is the proximity effect [11]: the gaps between the cuboids are very small and each gap receives an amount of secondary electrons from either side, so that the gap is accidentally exposed and thereby partially developed, as seen in fig. 1(a). On the other hand, a lower dose brings about underexposed patterns or bigger gaps. A precise tuning of the applied dose is thus needed, which would require a proximity-correcting software.

For the above reasons, we performed a negative exposure of the previous patterns on a positive resist (AR-P 671). In this way, the narrow gaps between the cuboids are exposed only once, minimizing the proximity effect. A double layer of positive resist was spin-coated and then baked at 160 °C for 5 min. In this case, the dose was $350\,\mu$C/cm^2. The development of the resist was then performed in a solution of diluted methylisobutyl ketone and isopropanol in a 1:3 ratio at room temperature. Afterwards, the pattern was transferred onto the Si layer via RIE with CF$_4$ gas, using a power of 80 W and a pressure of 1.06×10^{-4} mbar for 150 s. Finally, the samples were cleaned with acetone and oxygen plasma asher to remove any residual resist. The resulting cuboids, in fig. 1(b), exhibit nearly vertical side-walls and smooth surfaces undamaged by the etchant agents.

3. – Optical experiments

Figure 2(a) illustrates the optical experiment. A pulsed (160 fs duration, 80 MHz repetition rate) laser beam with peak frequency ω, corresponding to a $\lambda_{\mathrm{p}} = 1554$ nm wavelength, is loosely focused on the MS to a spot with a lateral size of $20\,\mu$m. The
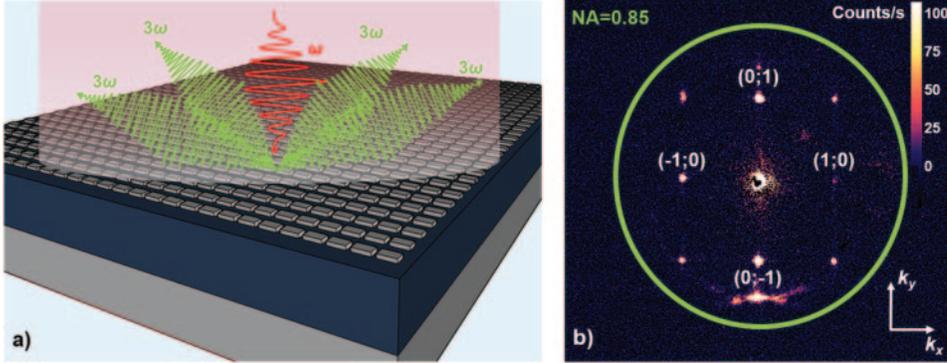
Fig. 2. – (a) Sketch of the optical experiment performed on a Si MS. (b) BFP image of the TH emission in the wavevector (k) space. The TH intensity is encoded in false colour according to the calibration bar (in counts/s). The green circle indicates the detection NA.

exciting field resonates with the magnetic quadrupole mode of the cuboids [9], thereby boosting the nonlinear conversion. The TH emitted at 3ω is collected by a 0.85 numerical aperture (NA) dry microscope objective in back-scattering configuration. The back focal plane (BFP) of the objective lens is imaged onto a charge-coupled device (CCD) camera, which records the emission in the direction space (fig. 2(b)). Thanks to the periodic arrangement of the cuboids, the TH emission is channeled into angularly narrow diffraction orders, arranged in a square lattice of period $\lambda/P = (1554\,\mathrm{nm}/3)/1065\,\mathrm{nm} = 0.49\,\mathrm{NA}$, corresponding to an emission angle of 51° for the lowest orders, $(\pm 1; 0)$ and $(0; \pm 1)$.

We described in detail this optical experiment in a recent work [9], with a focus on the polarization properties of the individual orders. Here, we concentrate instead on how the coupling to the excitation, and hence the overall efficiency of the TH conversion, can be optimized by adjusting the geometry. We therefore fabricated MSs of two different geometries ($L = 934\,\mathrm{nm}$, $W = 419\,\mathrm{nm}$, $P = 1019\,\mathrm{nm}$ and $L = 862\,\mathrm{nm}$, $W = 437\,\mathrm{nm}$, $P = 1064\,\mathrm{nm}$) to sustain a resonance at ω of different spectral width (having quality factors Q of about 400 and 100 respectively). Of each samples, we fabricated 4 additional copies, by dilating/shrinking the original geometry(L, W and P) by a scaling factor.

The resonant behaviour of the 10 fabricated geometries is illustrated in fig. 3(a) and (d), showing the internal electromagnetic energy $\mathcal{E}(\lambda) = \frac{\varepsilon}{2} \int_V |\vec{E}|^2 \, \mathrm{d}V$ localized in the volume V of the MS. $\mathcal{E}(\lambda)$ was simulated under a monochromatic plane wave excitation, with normal incidence onto the sample (*i.e.*, $k \parallel z$) and y polarization, that is, perpendicular to the long axis of the cuboids. The power spectrum of the laser source, $\mathcal{P}(\lambda)$, is described well by a Gaussian of FWHM = 16 nm and peak wavelength $\lambda_\mathrm{p} = 1554\,\mathrm{nm}$. In order to quantify the amount of exciting power coupled to the MS, let us define a figure of merit given by the excitation overlap to the resonance (EOR)

$$\mathrm{EOR} \equiv \int \mathcal{E}(\lambda)\,\mathcal{P}(\lambda)\,\mathrm{d}\lambda = \int \mathcal{E}(\lambda) \frac{1}{\sqrt{2\pi\sigma^2}} \exp\left[-\frac{(\lambda - \lambda_\mathrm{p})^2}{2\sigma^2}\right] \mathrm{d}\lambda \, , \text{ where } \sigma = \frac{\mathrm{FWHM}}{2\sqrt{2\log 2}}.$$

Since the TH power scales as the cube of the exciting power, we expect it to be proportional to $|\mathrm{EOR}|^3$. Such simulated value is compared to the measured TH power in fig. 3(b),(c),(e),(f). The EOR peaks for the samples with the design set of parameters, which was indeed adjusted to have the resonance at λ_p. The measured TH follows the trend of the EOR for the low-Q set, whereas for the high-Q set the largest geometries
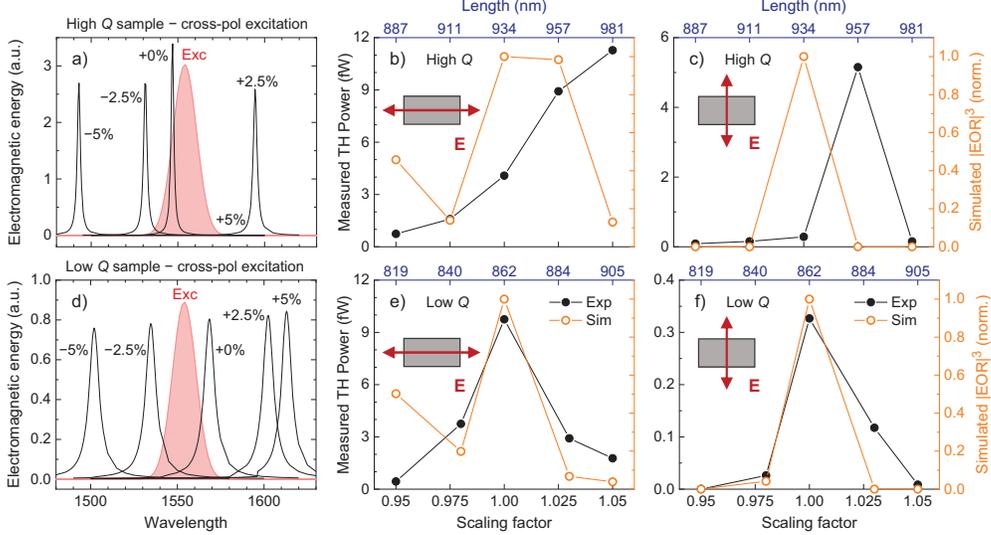
Fig. 3. – (a),(d) Electromagnetic energy in the MSs simulated as a function of the excitation wavelength, identified by their Q factor and in-plane scaling factors. The filled curve is the Gaussian spectrum of the experimental source. (b),(c),(e),(f) Measured TH power (black squares, left axes) and simulated EOR (red circles, right axes) emitted by the 10 studied MSs. The pump polarization with respect to the cuboids is indicated by sketches within each panel. (a)–(c) and (d)–(f) refer respectively to the high and low Q factor samples.

are the most efficient. We ascribe this discrepancy to systematic deviations of the fabricated geometry from the design one, resulting in a resonance shift from the intended frequency.

In conclusion, we studied TH generation and diffraction by a Si MS and highlighted the pivotal role of an effective coupling between the excitation and the localized modes. When engineering a resonant mode, one should strike a balance between a strong local field enhancement (*i.e.*, a high Q) and a good match to the bandwidth of the excitation.

REFERENCES

[1] SAIN B. *et al.*, *Adv. Photonics*, **1** (2019) 024002.
[2] CARLETTI L. *et al.*, *ACS Photonics*, **3** (2016) 1500.
[3] KOSHELEV K. *et al.*, *ACS Photonics*, **8** (2021) 102.
[4] FOROUZMAND A. *et al.*, *J. Opt.*, **18** (2016) 125003.
[5] BENALI A. *et al.*, *J. Phys.: Photonics*, **2** (2020) 015002.
[6] LÖCHNER F. *et al.*, *ACS Photonics*, **5** (2018) 1786.
[7] SHCHERBAKOV M. *et al.*, *Nano Lett.*, **15** (2015) 6985.
[8] GENEVET P. *et al.*, *Optica*, **4** (2017) 139.
[9] TOGNAZZI A. *et al.*, arXiv:2101.09187 (2021).
[10] STAUDE I. *et al.*, *Nat. Photonics*, **11** (2017) 274.
[11] MAILLY D. *et al.*, *Eur. Phys. J. ST*, **172** (2009) 333.